Applied Catalysis B: Environmental 110 (2011) 50–57

Contents lists available at SciVerse ScienceDirect

Applied Catalysis B: Environmental

journal homepage: www.elsevier.com/locate/apcatb

Carbon nanotube/titanium dioxide (CNT/TiO_2) core–shell nanocomposites with tailored shell thickness, CNT content and photocatalytic/photoelectrocatalytic properties

Ziyan Li [a], Bin Gao [a], George Zheng Chen [a], Robert Mokaya [b], Sotiris Sotiropoulos [c], Gianluca Li Puma [a,d,*]

[a] Department of Chemical and Environmental Engineering, The University of Nottingham, University Park, Nottingham NG7 2RD, United Kingdom
[b] School of Chemistry, University of Nottingham, University Park, Nottingham NG7 2LE, United Kingdom
[c] Physical Chemistry Laboratory, Chemistry Department, Aristotle University of Thessaloniki, Thessaloniki 54124, Greece
[d] Photocatalysis & Photoreaction Engineering, Department of Chemical Engineering, Loughborough University, Loughborough LE11 3TU, United Kingdom

ARTICLE INFO

Article history:
Received 21 April 2011
Received in revised form 31 July 2011
Accepted 18 August 2011
Available online 25 August 2011

Keywords:
CNTs
Nanotubes
Photocatalysis
Surfactant
Wrapping
Photo-oxidation
Nanostructure
Semiconductor
Photocatalytic
Photoelectrocatalysis

ABSTRACT

Combining carbon nanotubes (CNTs) with TiO_2 at the nano-scale level can promote the separation of the electron–hole charges generated upon irradiation. However, charge separation capability depends on the quality of the interfacial contact between CNTs and TiO_2, and on the morphological and surface properties of the nanocomposites. In this study, CNT/TiO_2 nanocomposites with tailored uniform core–shell coatings were fabricated from different titania precursors (titanium ethoxide (TEOTi), titanium isopropoxide (TTIP) and titanium butoxide (TBT)) by surfactant wrapping sol–gel method. This method produces a uniform and well-defined nanometer-scale anatase titania (TiO_2) layer on individual CNT (multi-walled), producing a mesoporous nanocomposite film. The composites were characterized by a range of analytical techniques including TEM, XRD, BET, TGA and UV–vis to reveal the textural, crystallographic and optical properties of the composites. The nanocomposites produced from the different Ti precursors exhibited significant differences in photocatalytic activity and photocurrent within the experimental range. A thinner TiO_2 layer provides shorter distance for electron transfer to the CNT core enhancing photocatalytic activity (degradation of methylene blue). However, higher CNT content in the composites correlates with higher photocurrents. It is shown that TiO_2 film thickness is the key factor controlling electron transfer and photocatalytic activity in CNT/TiO_2 nanocomposites with a core–shell structure, when the catalyst is applied in an irradiated slurry suspension. However, it is the electronic conductivity of the nanocomposite catalyst film, which increases with CNT content that controls the rate of electron removal from the photocatalyst when it is subject to an external positive bias in an appropriate photo-electrochemical cell. Overall, the CNT/TiO_2 composite prepared from TBT performed significantly better than those prepared from TEOTi and TTIP.

1. Introduction

The coupling of carbon nanotubes (CNTs) and titanium dioxide (TiO_2) has attracted much attention in the literature as a means for enhanced photo-induced catalysis for environmental and renewable energy applications, such as photocatalysis, photo-electro-catalysis, CO_2 photoreduction, hydrogen evolution, dye sensitized solar cells and sensor devices [1–10]. Combining CNTs with TiO_2 at the nano-scale level can promote the separation of the electron–hole charges generated upon irradiation [11]. Furthermore, CNTs can provide spatial confinement of TiO_2 and large supporting surface areas, leading to faster observed rates of redox reactions.

Many investigations have focused on material and photocatalytic/photo-electro-catalytic properties of heterogeneous non-uniform coatings of TiO_2 onto CNT, typically showing bare CNTs surfaces and random aggregation of TiO_2 onto the CNT surface. However, it is well known that the charge separation capability should depend on the quality of the interfacial contact between CNTs and TiO_2, and on the morphological and surface properties of the nanocomposites. Hence, tailored uniform core–shell coatings of TiO_2 on the CNTs surface should improve the transfer of photo-induced free electrons from the TiO_2 matrix to the CNTs and inhibit the recombination of photo-induced carriers through the formation of heterojunctions [12,13]. Core–shell structures with a semiconductor oxide coating of small and

* Corresponding author at: Photocatalysis & Photoreaction Engineering, Department of Chemical Engineering, Loughborough University, Loughborough LE11 3TU, United Kingdom. Tel.: +44 1509 222 510; fax: +44 1509 223 923.
E-mail address: g.lipuma@lboro.ac.uk (G. Li Puma).

0926-3373/$ – see front matter © 2011 Elsevier B.V. All rights reserved.
doi:10.1016/j.apcatb.2011.08.023

uniform thickness should provide the most efficient removal of photo-generated electrons since the probability of electron–hole recombination should depend solely on the thickness of the oxide layer over the entire length of the composite tubes. Such uniform coatings have been prepared by chemical vapour deposition, electro-spinning methods and more recently by modified sol–gel methods [1,11,14–17]. Carbon content, photon absorption, surface area, TiO_2 film morphology and crystallinity may affect the rate of charge separation, however, there is no clear evidence to suggest which of the above factors controls the rate of photogenerated hole and electron transfer.

In our previous studies [11,18] we have demonstrated the preparation of core–shell structured CNT/TiO_2 nanocomposites. Such prepared nanocomposites exhibited uniform shell thickness by a novel surfactant wrapping sol–gel method which resulted in composites with enhanced photocatalytic and photoelectrocatalytic activity compared to TiO_2 alone and/or to composites prepared by a conventional sol–gel method. However, we did not investigate the influence of TiO_2 shell (layer) thickness and conductivity on electron transfer in the composites and the resulting photocatalytic and photoelectrocatalytic properties. Furthermore, the use of these nanocomposites in either an irradiated slurry suspension or in an immobilized form as a photoanode may demand different tailoring properties for the composites.

In this study, we reveal new insights of the key factors controlling the photocatalytic and photoelectrochemical properties of CNT/TiO_2 composites prepared by the surfactant wrapping sol–gel technique. Particularly, we suggest that the key parameters that govern the composite behavior differ depending on whether the composite is used in a suspended photocatalytic system (a slurry suspension) or it is immobilized on a conductive support in a photo-electrochemical system (a photoanode). We show that the thickness of the TiO_2 layer and the conductivity of the composite (which increases with the CNT content) have profound effects on the photocatalytic and photoelectrocatalytic properties of the composites in each of the above applications.

2. Experimental

2.1. Synthesis of CNT/TiO_2 nanocomposites

CNT/TiO_2 nanocomposites were produced from raw multiwall CNTs from three different precursors, namely titanium ethoxide (TEOTi), titanium isopropoxide (TTIP) and titanium butoxide (TBT) by the surfactant wrapping sol–gel technique [11,18]. This simple technique, utilizing sodium dodecylbenzesulfonate (NaDDBS) as the CNT surface functionalizing agent (Fig. 1) provides a well defined, uniform, continuous, mesoporous TiO_2 (anatase) layer over the CNTs [11,18]. In a typical synthesis of CNT/TiO_2 nanocomposite, raw multiwall CNTs (10–30 nm in diameter, 5–15 μm in length, Shenzhen Nanotech Port Co. Ltd.) were dispersed into 0.5 wt% NaDDBS (Aldrich) aqueous solution (Millipore grade) and sonicated overnight. The concentration of CNTs in the dispersion was 14.5 g L^{-1}. The stable and well-dispersed CNTs suspension was then mixed with 20 mL ethanol (Acros, >95%, denat. with MEK) for 30 min to reach a uniform suspension. A predetermined amount (CNT/TiO_2 mass ratio = 0.9) of titanium precursor (TTIP, Fluka, purum; TBT, Fluka, purum; TEOTi, 99+%) was mixed with 15 mL ethanol and glacial acetic acid (Fisher, aldehyde free) under stirring for 30 min to form a clear solution. This solution was then added dropwise into the CNT suspension under vigorous stirring and the mixture was further stirred at room temperature for 2 h. Diluted ammonia aqueous solution (Fisher, 35%, S.G. 0.88) was then added dropwise to terminate the hydrolysis of the titanium precursor (pH 9) to form an amorphous TiO_2 shell supported over the CNT core (Fig. 1). 10 mL ethanol was added into the reaction system and stirring was maintained for another 30 min. The suspension was separated by three successive cycles of centrifugation and washing with ethanol. The sample was oven dried at 60 °C for 10 h, ground and calcined at 500 °C for 30 min to obtain crystalline CNT/TiO_2 core–shell nanocomposites. This calcination temperature was selected as a compromise between achieving a highly crystallized TiO_2 shell and avoiding significant loss of carbon from the core of the CNT/TiO_2 structure at higher temperatures (see TGA results). TGA of pristine CNT showed a negligible mass loss at 500 °C [11] but above this temperature a progressively increasing rate of mass loss was observed up to the combustion point of 653 °C. The intactness of the CNT structure after calcination at 500 °C was also confirmed by TEM analysis of the composites.

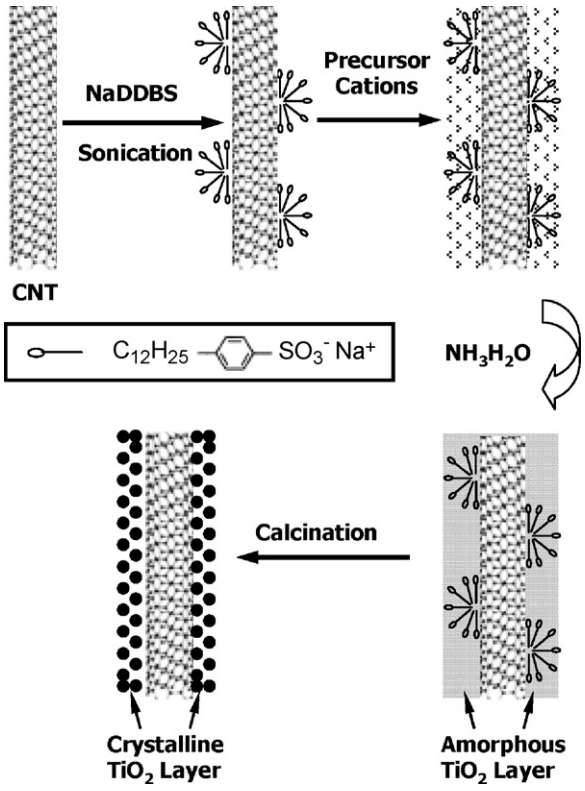

Fig. 1. Synthetic scheme for the preparation of CNTs/TiO_2 nanocomposites by the surfactant wrapping sol–gel method, in the presence of sodium dodecylbenzesulfonate (NaDDBS).

2.2. Catalyst characterization

The crystallinity of the CNT/TiO_2 composites was characterized by powder X-ray diffraction (XRD). The XRD patterns were recorded in a Philips EXPERT θ–2θ X-ray diffractometer with Cu Kα radiation (α = 1.54060 Å) from 10° to 80° 2θ at a scanning speed of 0.02° s^{-1}. The X-ray tube voltage and current were set at 40 kV and 40 mA, respectively. The crystallite size was estimated from the line broadening of anatase TiO_2 (2 0 0) reflection plane (2θ = ca. 48.1°), where there is negligible interference from CNTs.

Nitrogen sorption isotherms and textural properties of the materials were determined in a conventional volumetric technique at 77 K using nitrogen by a Micrometrics ASAP 2010 sorptometer. Before analysis, the samples were oven-dried at 60 °C and evacuated overnight under vacuum. The surface area was calculated using Brunauer–Emmett–Teller (BET) surface analysis based on adsorption data in the partial pressure (P/P_0) range

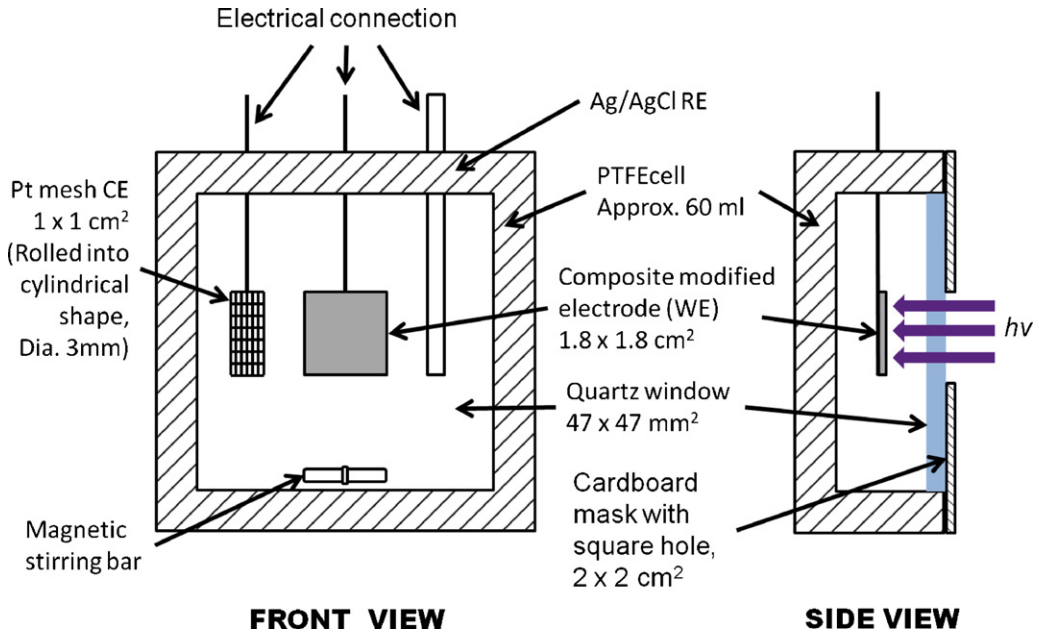

Fig. 2. Schematic setup of the photoelectrochemical cell used for photo-current measurement.

0.05–0.35. The total pore volume was determined by the amount of nitrogen adsorbed at $P/P_0 = 0.995$. The average pore size was obtained from the adsorption data by Barrett–Joyner–Halenda (BJH) porosity model.

A Pyris 1 TGA thermogravimetric analyzer was used for the analysis of the composition of the sample. 1 mg of the sample composite was heated from 50 °C to 950 °C with a heating rate of 10 °C min^{-1} under an airflow of 10 mL min^{-1}.

Transmission electron microscopy (TEM) and corresponding energy dispersive X-ray (EDX) were carried out on a JEM-2010F and a JEM-2000FX at 200 kV. The specimens for TEM imaging were prepared by suspending solid samples in ethanol with 15 min ultrasonication.

UV–vis absorption spectra of the catalysts aqueous suspensions were measured in a UV–vis spectrometer, Jenway 6400. Catalyst suspensions made in Millipore grade water at a concentration of 0.1 g L^{-1} were scanned from 300 nm to 450 nm at 5 nm interval.

2.3. Photocatalytic activity

The photocatalytic activities of the nanocomposites were monitored from the results of the photodegradation of methylene blue (MB) (Aldrich) (10 mg L^{-1} initial concentration in a 200 mL Millipore grade aqueous suspension containing 0.1 g L^{-1} of catalyst). The dark adsorption time was 1 h. The reactions were carried out for 3 h under stirring in a Pyrex circular vessel. The reactor was irradiated by three UV-A lamps (Philips TL 8W/08 F8T5/BLB, 1.2W UV-A output) located directly above the vessel at a distance of 6 cm from the surface of the liquid. The lamps emitted a minute fraction of the total radiation at 324 and 325 nm, the rest between 342 and 400 nm with a maximum irradiance peak at 365 nm. The lamp axes were separated by 3 cm. The average incident photon flux (between 324 nm and 384 nm) at the free surface of the liquid was 24 W m^{-2}. It was determined with a Microprocessor-Controlled Radiometer (Cole Parmer, 97503-00) fitted with a 365 nm sensor and using Eq. (1), where I_{sensor} is the incident radiation measured with the radiometer, P_λ is the relative spectral response of the 365 nm sensor, W_λ is the radiant power of the lamp at wavelength λ, 324 nm is the minimum wavelength emitted by the lamp and 384 nm is the highest wavelength that can photoactivate the immobilized anatase TiO_2:

$$I = I_{sensor} \frac{\int_{324\,nm}^{384\,nm} W_\lambda d\lambda}{\int_{324\,nm}^{384\,nm} W_\lambda P_\lambda d\lambda} \quad (1)$$

The concentration of MB of the samples collected at regular intervals, through a 0.45 μm membrane filter, was measured by a Shimadzu UV-mini 1240 UV-vis spectrophotometer. The membrane filter did not adsorb MB.

2.4. Photocurrent density measurements

The composite-modified electrode was prepared by the following method. A titanium (Ti) foil substrate (1.8 cm × 1.8 cm, 0.1 mm thickness, purity 99.6+%, Advent research material) was first heated to 750 °C in air (10 °C min^{-1}) for 60 min to form a compact layer of TiO_2 insulation on the surface. The Ti foil was then polished by medium- and fine-grade sandpaper to reveal the metal surface on one side. This base electrode was then washed in acetone and ultrapure water under sonication and air-dried before use. 1 mg of the calcined CNT/TiO_2 composite was uniformly suspended in 0.5 mL ultrapure water by sonication, and was drop cast on the metal electrode surface. The electrode was dried at 40 °C for 6 h in air and heat-treated at 300 °C for 15 min to improve the adhesion between the thin film and substrate. During this short heat treatment period insignificant modification of the composite microstructure and crystallinity was to be expected. TGA of the calcined composites showed negligible mass loss at 300 °C and the short treatment time and modest temperature can be expected to have little effect on crystal size, surface area and porosity. The CNT/TiO_2 modified electrode was then ready for use.

A three-electrode system was set up as in the scheme shown in Fig. 2 to measure the photo-current generated by the composite-modified electrode. It included the titanium plate supported CNT/TiO_2 working electrode, a platinum mesh counter-electrode and a Ag/AgCl reference electrode. The stability of the reference electrode was maintained by a long portion (salt bridge) that contained only the electrolyte solution. The Ag/AgCl electrode was not irradiated by the UV light beam. The photo-current

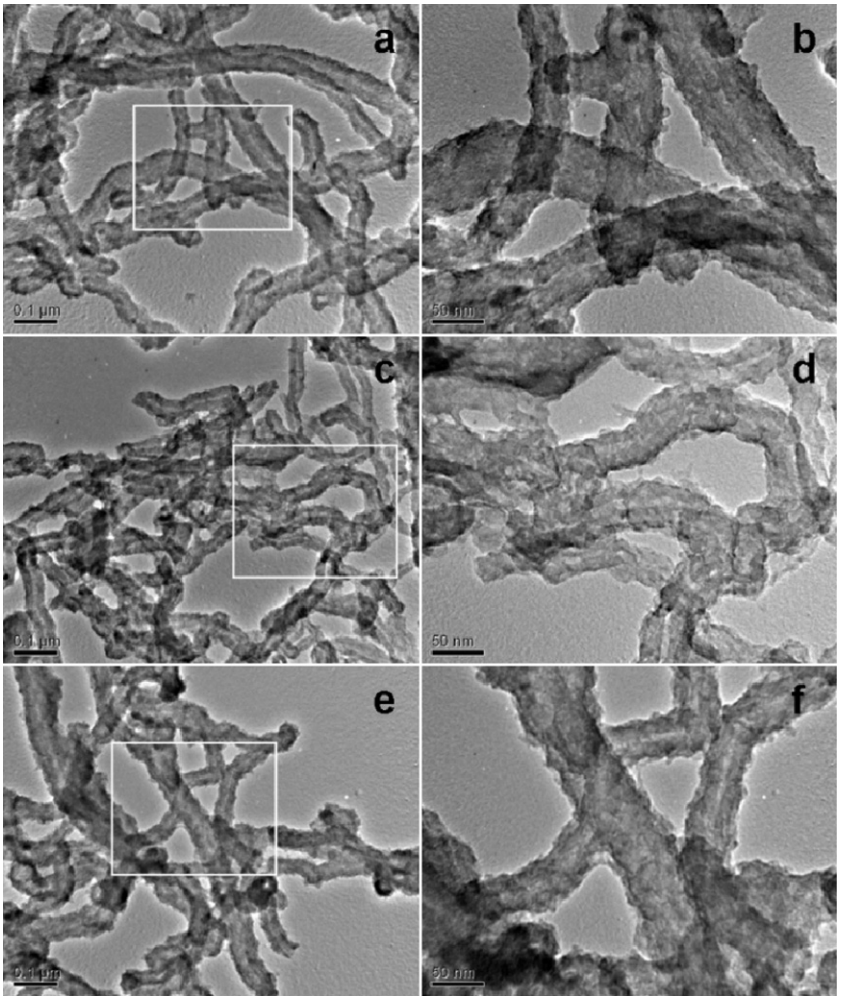

Fig. 3. TEM images of CNT/TiO_2 nanocomposites prepared from pristine CNTs with different TiO_2 precursors before calcination: (a and b) TTIP; (c and d) TBT; (e and f) TEOTi. The images on the right have higher resolutions.

was recorded using the chrono-amperometry method (0.1 s interval time) on a Autolab (PGSTAT30, Eco Chemie [now Metrohm]), which at the same time also provided constant external bias (0.6 V) to the system. Such a potential was selected based on cyclic voltammetry in the dark and under illumination to avoid water electrochemistry to take place. Further, it is well-known that at the potential of +0.6 V vs. Ag/AgCl in neutral solutions, the photocurrent response of particulate TiO_2 electrodes (either of anatase or rutile structure or of their mixtures) reaches a maximum-limiting value limited by charge carrier migration [11]. Hence this choice ensures the maximum photoelectrochemical charge separation that is also not very sensitive to potential fluctuations since it lies well into the limiting photocurrent vs. potential plateau.

One 8 W Philips UV-C lamp (1.2 W UV-C output) emitting monochromatic radiation at 253.7 nm was used to irradiate the electrode. The photon flux measured at the electrode plane surface by a calibrated microprocessor-controlled radiometer (Cole–Parmer) fitted with a 253.7 nm UVC sensor was 92 W m^{-2}.

In a typical experiment, the cell contained 50 mL methylene blue aqueous solution (5 ppm) and 0.1 M NaCl supporting electrolyte. The electrodes were subject to 1-h dark adsorption. UV irradiation cycles started after the photocurrent reached steady state.

All experiments were performed in triplicate to ensure the reproducibility in the composite synthesis, catalyst activity and characterization.

3. Results and discussion

3.1. Characterization of CNTs/TiO_2 nanocomposites prepared from different Ti precursors

The TEM images of the uncalcined composites, shown in Fig. 3, confirmed the existence of a continuous thin layer coating covering the entire surface of CNTs. The diameter of the raw CNTs was 10–30 nm. The thickness of the TiO_2 layer was estimated to be 5–15 nm while the average diameters of the composite tubular structures of the uncalcined samples were 40 ± 11 nm for CNT/TiO_2 (TBT), 49 ± 10 nm for CNT/TiO_2 (TTIP) and 49 ± 12 nm for CNT/TiO_2 (TEOTi). The average diameters were estimated from enlargements of TEM images by considering each tube section and averaging the measurements. The TBT-derived composite (Fig. 3c and d) presented a coating on CNTs with a thinner layer compared to those observed for the other two composites. The TEM images of the calcined composites (500 °C for 30 min) shown in Fig. 4 confirmed the presence of untangled composites made by a continuous and uniform thin layer of crystalline TiO_2 covering the entire surface of the CNTs. The images on the right hand side in Fig. 4 (b, d, and f) show the rare appearance of bare CNTs in the composites which confirmed the intactness of the CNT tubular structure after the calcination. They also show that the TiO_2 overlayer (shells) over the CNTs base material (cores) are thinner in the TBT-derived composite and that thicker TiO_2 shells were formed in the composites

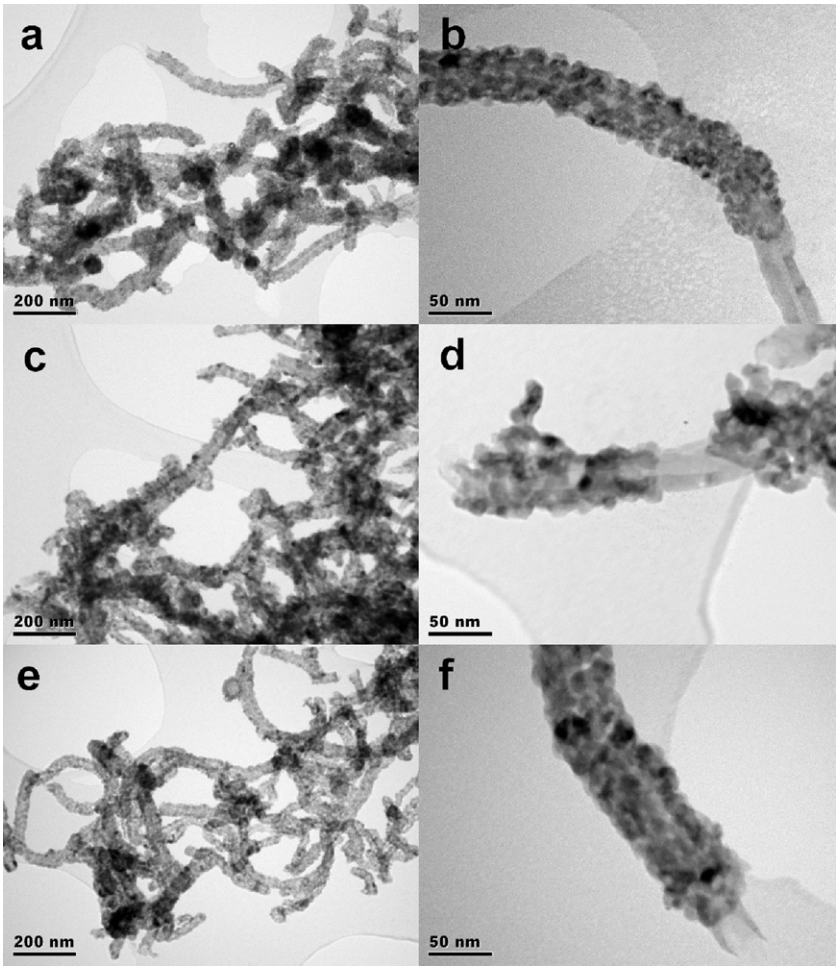

Fig. 4. TEM images of calcined CNT/TiO_2 nanocomposites prepared from pristine CNTs with different TiO_2 precursors: (a and b) TTIP; (c and d) TBT; (e and f) TEOTi. Images on right hand side show comparisons in thickness of TiO_2 layer with rare appearance of bare CNT.

prepared from TTIP and TEOTi. This was possible because the morphology of TiO_2 was greatly dependent on the nature of the alkoxyl ligands, e.g. steric structure and alkyl chain length of the precursors and their effect on the rate of hydrolysis to TiO_2 [20,21].

XRD patterns (Fig. 5) of the sintered composites suggested the formation of pure anatase crystallites. No characteristics peaks of CNTs were found in the spectra of the composites in the range investigated. This may be attributed to the overlap of the intense peaks of the CNTs (0 0 2) and anatase (0 0 1) reflections, as the difference in mass between CNTs and TiO_2 is relatively large.

Porosity analysis revealed quantitative differences in textural properties amongst the three composites which showed type IV isotherms, indicating the presence of mesopores in the particle matrix (Fig. 6). Table 1 presents the surface area and pore volume

Table 1
BET surface area and pore volume of CNTs, pure TiO_2 and of CNT/TiO_2 composites from different titanium precursors. Crystal sizes of TiO_2 and composites.

	SA ($m^2\ g^{-1}$)[a]	V_{pore} ($cm^3\ g^{-1}$)[a,b]	d_{TiO_2} (nm)[c]
Raw CNTs	264	2.42	
TiO_2	197 (79)	0.14 (0.13)	15.3
CNT/TiO_2 (TTIP)	230 (120)	0.23 (0.19)	5.1
CNT/TiO_2 (TBT)	151 (93)	0.16 (0.15)	8.6
CNT/TiO_2 (TEOTi)	231 (133)	0.21 (0.20)	6.7

[a] Data in parenthesis were obtained after sintering at 500 °C for 30 min.
[b] Total pore volume adsorbed at a relative pressure of 0.995 for N_2 at 77K.
[c] d_{TiO_2} is the calculated TiO_2 crystal size from XRD spectra of calcined samples.

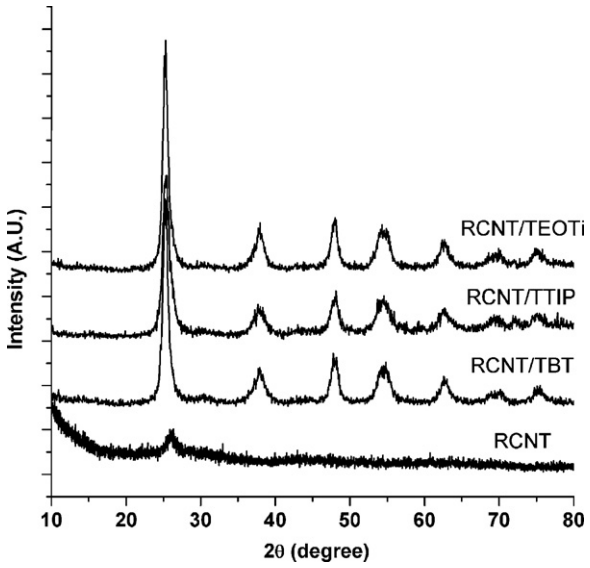

Fig. 5. XRD spectra of CNT and of calcined CNT/TiO_2 nanocomposites revealing the formation of anatase.

of various materials, including raw CNTs, pure TiO_2 and CNT/TiO_2 composites from different precursors. The lower surface area and pore volume of the composites, compared with that of pure CNTs, indicate that the presence of a TiO_2 layer blocked or filled up

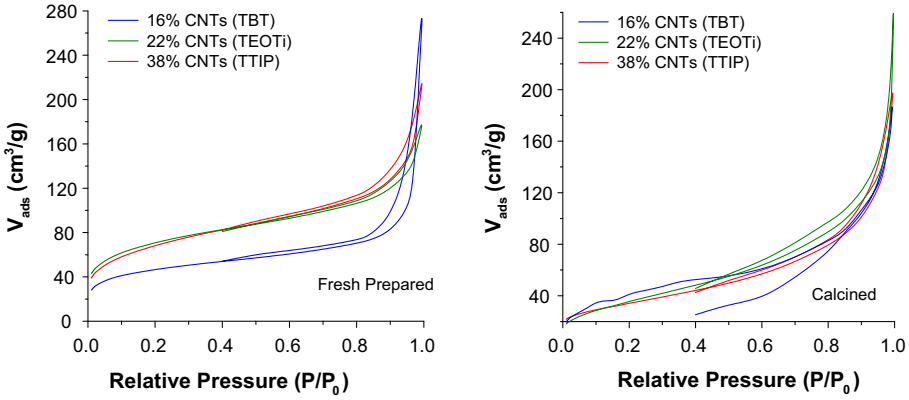

Fig. 6. N_2 adsorption–desorption isotherms of uncalcined (left) and calcined (right) CNT/TiO_2 composites.

gaps between the CNTs as well as partially clogged the nanotube openings. Conversely, the presence of CNTs enhanced the textural properties of the composites compared to pure TiO_2 aggregated particles, by providing an open structure and high surface area support for the formation of the TiO_2 film. The decrease of surface area after calcination can be attributed to shrinkage of the relatively porous coating because of heat-induced crystallization. The composites prepared from TTIP and TEOTi had similar properties while CNT/TiO_2 (TBT) showed significantly lower surface area, pore volume and larger crystal size (Table 1) possibly due a more compact TiO_2 shell compared to the specimens prepared from TTIP and TEOTi. This is consistent with differences in TiO_2 coating thickness and morphology observed in the TEM images. The crystal size of 100% TiO_2 was significantly larger than the crystals of the CNT/TiO_2 composites implying that the spatial confinement of the CNT scaffold leads to smaller TiO_2 crystals which in turn results in larger composite surface areas compared to the specimen with 100% TiO_2.

The thermal gravimetric analysis (TGA) data presented in Fig. 7 provided direct information on carbon nanotube CNT content of the composites, as well as, possible C-doping of TiO_2. The uncalcined composites revealed an initial weight loss event between 50 and 500 °C, due to the removal of adsorbed water and disintegration of amorphous carbon impurities, while calcined analogues exhibited negligible weight loss up to 500 °C. Between 550 and 750 °C both calcined and uncalcined composites showed significant weight losses due to the decomposition of CNTs, as confirmed by TGA experiments on uncoated CNTs [11]. The constant weight registered beyond 750 °C suggested that the CNTs were completely burnt off, leaving only material which did not change in weight below 1000 °C. These final weight percentages (at ca. 750 °C) represent the quantity of TiO_2 and of any C incorporated into it, while the weight loss between 550 and 750 °C represents the CNT content. The CNT content in calcined samples followed the order CNT/TiO_2 (TBT) – 16% < CNT/TiO_2 (TEOTi) – 22% < CNT/TiO_2 (TTIP) – 38%. All the calcined composites had less than the expected 47% CNT content based on material balance in the preparation process. This, together with the fact that no CNT thermal decomposition has been observed at the calcination temperature [11] points to the transfer-doping of elemental C from the CNT substrate into the TiO_2 coating or/and lattice [22–26]. Additional evidence supporting this effect can be found in the TGA curves of the thicker uncalcined samples (from TTIP and TEOTi precursors) that give an estimated ca. 41% weight loss between 500 and 1000 °C which is very close to the expected 47%. The thin sample from TBT however still shows a smaller loss of ca. 21%, presumably due to more effective doping occurring below 500 °C, even during the heating of the TGA experiment. Following this reasoning, the C incorporation/doping trend for calcined samples is TBT > TEOTi > TTIP and this should be attributed to different morphology, compactness and crystallinity of TiO_2 coatings as a function of precursor type [20,21]. Incidentally, lower levels of CNT and higher levels of C doping are observed for the thinner coating sample (TBT) and for the originally less porous samples (TTIP and TEOTi – see porosity results for as-prepared samples in Table 1).

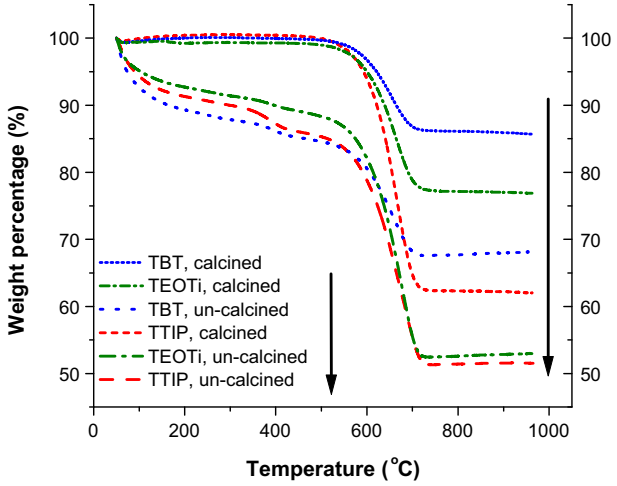

Fig. 7. TGA profiles of calcined and uncalcined CNT/TiO_2 composites prepared from various titanium precursors. Heating was at constant ramp rate of 10 °C min^{-1} in air. Preheated at 50 °C for 10 min.

3.2. *Photocatalytic activity of CNTs/TiO_2 nanocomposites prepared from different Ti precursors*

Control experiments showed that UV-A irradiation with no catalyst and catalyst (composite or pure TiO_2) without irradiation could not degrade methylene blue. The photocatalytic activity of the composites for the degradation of methylene blue (MB) (Fig. 8) was tested in an irradiated suspension of composites. Fig. 8a shows the conversion of MB to follow the sequence CNT/TiO_2 (TBT) > CNT/TiO_2 (TEOTi) > CNT/TiO_2 (TTIP) ≈ TiO_2. It is noteworthy that this order follows the opposite trend as that of the CNT content. The differences in photocatalytic activity amongst the specimens cannot be assigned merely to differences in photon absorption efficiency since the absorbances of the CNT/TiO_2 suspensions were similar within the radiation spectrum (320–400 nm) of the UV lamp (Fig. S1, Supplementary Data). One should notice the significant absorbance of the samples in the near-visible end of the spectrum, characteristic of C-doped TiO_2 [22–26], but longer wavelengths activity is not expected to affect the results of this study since the

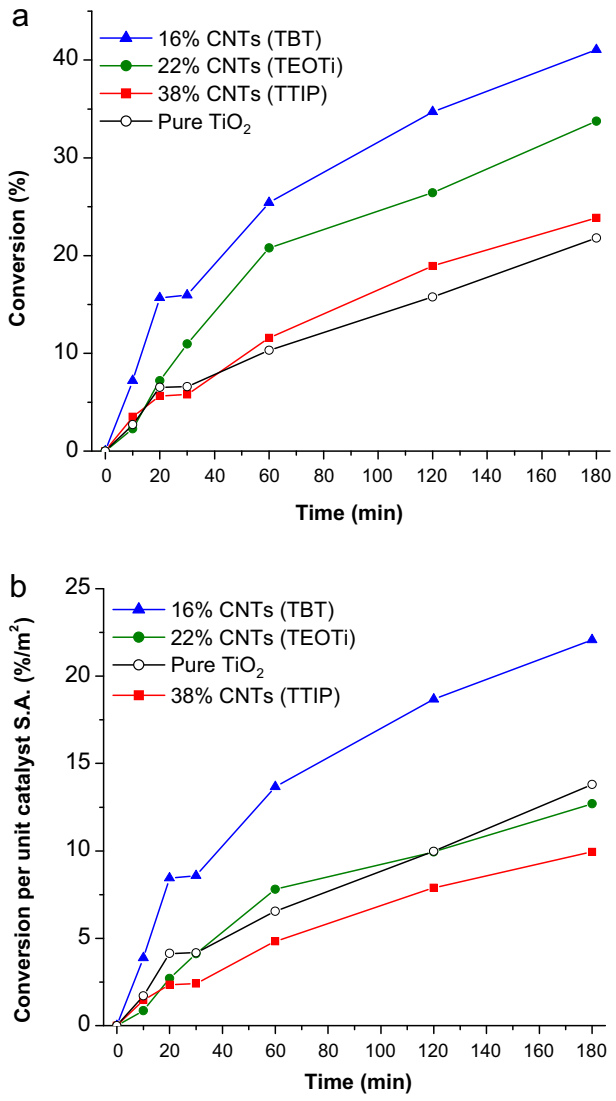

Fig. 8. Photocatalytic degradation of methylene blue (a) and conversion based on catalyst surface area (b) in the presence of CNT/TiO_2 composites with different carbon content, prepared from various precursors. UVA irradiation started after 1 h dark adsorption–desorption equilibrium. Total catalyst concentration = 0.1 g L^{-1}.

UVA lamp used emitted only a tiny part of its power in that region. Also, the photon penetration depth at 348 nm of polycrystalline TiO_2 is about 0.1 μm [27] and for mesoporous TiO_2 films will be significantly higher than 0.1 μm [28]. Therefore, the entire TiO_2 porous layer of 5–15 nm in thickness covering the CNT support, was fully irradiated by UVA photons and this implies that the entire mass of TiO_2 was photoactive. As a result, negligible transversal gradients in the rate of photon absorption by the TiO_2 layer had to be expected. The apparent, overall, activity of the CNT/TiO_2 composites shown in Fig. 8a was then normalized against the total surface area of the TiO_2-coated catalyst (Fig. 8b), calculated from the BET specific surface area after calcination (Table 1) multiplied by the mass of the catalyst used (0.1 g L^{-1} × 0.2 L = 0.02 g). The resulting conversion-per m^2-of catalyst is then indicative of the intrinsic photocatalytic activity of each catalyst. In such representation the profiles for the thick coating TEOTi and TTIP precursor catalysts were not better than that of the plain TiO_2 catalyst, indicating that the beneficial effect of the CNT in their overall activity (as depicted in Fig. 8a) was simply an increased surface area effect of the support. In contrast, the thin coating TBT precursor composite exhibited a significantly higher intrinsic activity. It is noteworthy to observe that the composites activities appear to be related to the thickness of the TiO_2 layer and not so much on CNT content or C-doping (if the last two parameters were critical then the TEOTi precursor – 22% CNT composite should show behavior closer to that of the TBT precursor – 16% CNT composite). This structure–property relationship can be rationalized as a reduction of photogenerated electron–hole recombination rates when the former can reach the CNT core through a relatively short travelling distance. We can thus conclude that the activity per unit surface area appears to be independent on the amount of CNTs, which only act as electron sinks in a photocatalytic system.

3.3. Photoelectrocatalytic activity of CNTs/TiO_2 nanocomposites prepared from different Ti precursors

When the composites are immobilized on an electrode, the anodic photocurrent generated upon irradiation of the CNT/TiO_2 photocatalyst film under the simultaneous application of a positive bias, relates to the ability of the catalyst to shuttle away photo-excited electrons through the external circuit of an appropriate electrochemical cell. In other words, electrochemically assisted photocatalysis is an eloquent way to minimize recombination rates, provided that the system possesses sufficient conductivity for the effective application of an external bias. It is also generally accepted that the photocurrent observed upon illumination of small TiO_2-based photoanodes can be correlated to the activity of the material in bulk photoelectrocatalytic destruction of organics [11,19,29]. However, the correlation of the photocurrent with the photocatalytic activity of the material under open circuit conditions is not straightforward and conflicting results have been obtained [11,26]. The composite modified electrodes in a photo-electrochemical cell (Fig. 2) under an external bias were prompt in generating photocurrent with a reproducible response to the on–off cycles of irradiation (Fig. 9). The results show that photocurrent density correlates in the same ascending order as the CNT content of the composites. To account for any surface area effects and obtain the intrinsic photoelectrocatalytic activity of the material, the photocurrents were normalized again per catalyst surface area (Fig. 9b), assuming that all BET surface area was in contact with/wetted by the electrolyte and hence accessible to (photo)electrochemistry. Even after correction for surface area differences the photocurrent trend remains the same i.e. 38% CNT/TiO_2 (TTIP) > 22% CNT/TiO_2 (TEOTi) > 16% CNT/TiO_2. In our previous study [11] we have shown CNT/TiO_2 composites photocurrents up to 5-fold higher than the photocurrents obtained with the electrode loaded with TiO_2. The CNTs are believed to play an important supportive role in electron transfer under external bias, since an extended CNT network ensures higher electronic conductivity of the composite electrode, a more efficient application of the electric field and hence faster removal of electrons from the composite layer towards the Ti electrode substrate and the external circuit. Therefore, in the case of photocurrents and photoelectrocatalytic activity, the thickness of the TiO_2 layer is not critical since charge separation is not driven by spontaneous transfer of electrons to CNT but by their migration to the anode collector due to the effective application of an external field to the photocatalyst via the extensive conductive network of CNTs. However, the observed photoelectrocatalytic trend is not reflected in the corresponding photocatalytic activity in irradiated slurry suspensions and, in fact, the results in Fig. 8 show the opposite trend. This suggests that the key parameters that govern the composite behavior differ in a suspended photocatalytic system from a photo-electrochemical system in which the CNT/TiO_2 composites are immobilized on a conductive support. The thickness of the TiO_2 layer dominates the transport of electrons towards the CNTs core when the catalyst is applied in a slurry suspension, and the CNTs acts as an electron sink. However, it is the conductivity of

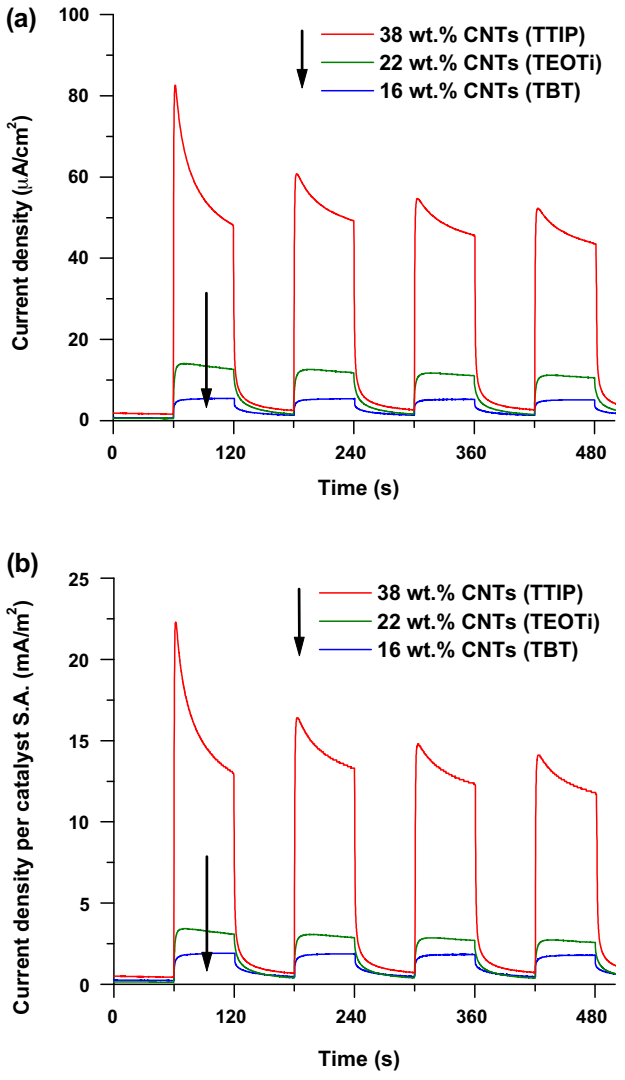

Fig. 9. Photocurrent density profile in response to cyclic on–off irradiation in 5 mg L^{-1} MB, 0.1 M NaCl solution, recorded on CNT/TiO_2 electrode (Ti base) with Pt mesh counter electrode. 0.6 V constant bias vs. Ag/AgCl. UVC (253.7 nm) intensity = 92 W m^{-2}. Surface area of electrode = 1.8 cm × 1.8 cm. CNT/TiO_2 loading = 1 mg.

an immobilized catalyst film (which increases with CNT content) that controls the effective application of an external bias and via that the rate of electron removal.

4. Conclusions

This study has demonstrated that different titania precursors lead to differences in the thickness of the TiO_2 layer and in the CNT contents of the composites prepared by the surfactant wrapping sol–gel method. This synthesis method produces entangled and core–shell structured CNT/TiO_2 nanocomposites which after calcination are made of well crystallized anatase titania covering the entire surface of individual CNTs. A thinner TiO_2 layer as obtained from using titanium butoxide as the Ti precursor provides a shorter distance for electron transfer under open circuit conditions, which enhances the photocatalytic activity in a slurry suspension. On the other hand, the titanium isopropoxide precursor produces a composite containing a higher CNT content which correlates with higher photocurrent densities of the immobilized composite when operated as the photoanode of a photoelectrocatalytic cell. These considerations would be valuable for tailoring CNT/TiO_2 nanocomposites to specific technological applications in the environmental and renewable energy sectors. The differences in the morphology and thickness of the TiO_2 shell is greatly dependent on the rate of hydrolysis which in turns depends on the nature of the alkoxyl ligands, e.g. steric structure and alkyl chain length, of the precursors.

Acknowledgements

This work was supported by the NATO grant CBP.EAP.SFPP 982835 and also by E.ON AG as part of the E.ON International Research Initiative: Nanotechnologies for Energy 2009 and Energy Storage 2007. Responsibility for the content of this paper lies with the authors.

Appendix A. Supplementary data

Supplementary data associated with this article can be found, in the online version, at doi:10.1016/j.apcatb.2011.08.023.

References

[1] S. Aryal, C.K. Kim, K.W. Kim, M.S. Khil, H.Y. Kim, Mater. Sci. Eng. C 28 (2008) 75.
[2] L. Chen, B.L. Zhang, M.Z. Qu, Z.L. Yu, Powder Technol. 154 (2005) 70.
[3] J. Cho, S. Schaab, J.A. Roether, A.R. Boccaccini, J. Nanoparticle Res. 10 (2008) 99.
[4] C.G. Silva, J.L. Faria, Appl. Catal. B: Environ. 101 (2010) 81.
[5] X.H. Xia, Z.H. Jia, Y. Yu, Y. Liang, Z. Wang, L.L. Ma, Carbon 45 (2007) 717.
[6] B. Liu, H.C. Zeng, Chem. Mater. 20 (2008) 2711.
[7] Y. Yu, J.C. Yu, C.-Y. Chan, Y.-K. Che, J.-C. Zhao, L. Ding, W.-K. Ge, P.-K. Wong, Appl. Catal. B: Environ. 61 (2001) 1.
[8] B. Ahmmad, Y. Kusumoto, S. Somekawa, M. Ikeda, Catal. Commun. 9 (2008) 1410.
[9] T.Y. Lee, P.S. Alegaonkar, J.-B. Yoo, Thin Solid Films 515 (2007) 5131.
[10] M. Sánchez, R. Guirado, M.E. Rincón, J. Mater. Sci.: Mater. Electron. 18 (2007) 1131.
[11] B. Gao, C.A. Peng, G.Z. Chen, G. Li Puma, Appl. Catal. B: Environ. 85 (2008) 17.
[12] H. Yu, X. Quan, S. Chen, H. Zhao, J. Phys. Chem. C 111 (2007) 12987.
[13] P. Brown, K. Takechi, P.V. Kamat, J. Phys. Chem. C 112 (2008) 4776.
[14] S. Guo, S. Dong, E. Wang, Small 4 (2008) 1133.
[15] A. Jitianu, T. Cacciaguerra, R. Benoit, S. Delpeux, F. Beguin, S. Bonnamy, Carbon 42 (2004) 1147.
[16] H. Yu, X. Quan, S. Chen, H. Zhao, Y. Zhang, J. Photochem. Photobiol. A: Chem. 200 (2008) 301.
[17] J. Li, S. Tang, L. Lu, C.Z. Hua, J. Am. Chem. Soc. 129 (2007) 9401.
[18] B. Gao, G.Z. Chen, G. Li Puma, Appl. Catal. B: Environ. 89 (2009) 503.
[19] I. Mintsouli, N. Philippidis, I. Poulios, S. Sotiropoulos, J. Appl. Electrochem. 36 (2006) 463.
[20] V. Barlier, V. Bounor-Legaré, G. Boiteux, J. Davenas, D. Léonard, Appl. Surf. Sci. 254 (2008) 5408.
[21] M. Crişan, A. Brăileanu, M. Răileanu, D. Crişan, V. Teodorescu, R. Bîrjega, V. Marinescu, J. Madarász, G. Pokol, J. Thermal Anal. Calorim. 88 (2007) 171.
[22] S.H. Kang, J.-Y. Kim, Y.-K. Kim, Y.-E. Sung, J. Photochem. Photobiol. A: Chem. 186 (2007) 234.
[23] A.W. Morawski, M. Janus, B. Tryba, M. Toyoda, T. Tsumura, M. Inagaki, Polish J. Chem. Technol. 11 (2009) 46.
[24] K. Shankar, J.I. Basham, N.K. Allam, O.K. Varghese, G.K. Mor, X. Feng, M. Paulose, J.A. Seabold, K.-S. Choi, C.A. Grimes, J. Phys. Chem. C 113 (2009) 6327.
[25] C. Di Valentin, G. Pacchioni, A. Selloni, Chem. Mater. 17 (2005) 6656.
[26] H.J. Yun, H. Lee, J.B. Joo, N.D. Kim, J. Yi, Electrochem. Commun. 12 (2010) 769.
[27] W. Choi, J.Y. Ko, H. Park, J.S. Chung, Appl. Catal. B: Environ. 31 (2001) 209.
[28] N.J. Peill, M.R. Hoffmann, Environ. Sci. Technol. 29 (1995) 2974.
[29] J. Georgieva, S. Sotiropoulos, S. Armyanov, N. Philippidis, I. Poulios, J. Appl. Electrochem. 41 (2011) 173.